Energy Advances

ROYAL SOCIETY OF CHEMISTRY

PAPER

View Article Online
View Journal | View Issue

Cite this: *Energy Adv.*, 2026, 5, 56

Enhancing the durability of Au-coated Ti porous transport layers (PTLs) with a thin Pt top layer for PEM water electrolyzer applications

Sukhvant Singh, Aditya Singh, Muhammad Azhar Iqbal and Samaneh Shahgaldi *

Received 17th September 2025,
Accepted 27th November 2025

DOI: 10.1039/d5ya00274e

rsc.li/energy-advances

The porous transport layer (PTL) is an integral component of the proton exchange membrane water electrolyzer (PEMWE), ensuring the supply of water, electrical conduction, and the removal of produced oxygen. The applied positive potential and acidic nature of the proton exchange membrane (PEM) in the PEMWE lead to an acidic environment, which promotes the formation of passivated TiO_x on the surface of the Ti PTL. The limited conductivity of TiO_x results in an increase in contact resistance and cell voltage. The precious metal coatings prevent TiO_x formation, ensure low interfacial contact resistance (ICR), and provide long-term stability. In this work, a durable bilayer coated Ti PTL was prepared by applying a thin Pt sputtered coating onto Au-electroplated PTL. The bilayer coating of Au/Pt reduced the loading of precious metals to a low level (overall 0.14 mg cm^{-2}) while exhibiting outstanding corrosion resistance and cell performance. The coated Pt layer with 0.06 mg cm^{-2} loading on Au coated Ti PTL exhibited a stability number 50 times higher than that of Ti PTL coated with Au alone. The balanced residual shear stress at the Au/Pt interface assisted to improve the charge transfer resistance against acid based corrosive environment. Employing the TiH/Au/Pt-0.06 coating on the Ti-PTL, a PEMWE cell performance of 1.716 V at 2.0 A cm^{-2} was achieved at 80 °C under ambient pressure.

1. Introduction

Due to ongoing initiatives to cut carbon emissions, hydrogen is set to play an increasingly vital role in energy networks, with worldwide demand expected to surge significantly.[1] Hydrogen produced through electrolysis is considered a viable potential option due to its high energy content and reputation as a sustainable fuel.[2–6] The electrical form of energy can be effectively transformed into the chemical form of energy using the water electrolysis process, where water molecules are split into their elemental components, oxygen and hydrogen, using a PEMWE cell. At the core of the PEMWE single cell is the membrane electrode assembly (MEA), a crucial component that facilitates the water-splitting reactions. The MEA is tightly sandwiched between two essential layers: a porous transport layer (PTL), typically composed of metal, which allows for efficient movement of water and gases, and a gas diffusion layer (GDL), usually made from carbon-based materials, designed to evenly distribute gases across the catalyst surface. These components are held together and supported by bipolar plates (BPPs), which not only provide mechanical stability but also help in current collection and gas separation, ensuring the system operates with high efficiency and durability.[2,7–11] In the presence of externally applied electrical power, water molecules undergo oxidation and yield oxygen and protons as well as electrons at the anode side of the PEMWE cell. These produced protons then migrate through the solid electrolyte (proton exchange membrane) to the cathode side and react with electrons to produce molecular hydrogen gas.[10] Under standard conditions, the thermo-neutral voltage at the anode of a PEMWE cell is approximately 1.480 V; however, the actual operating voltage may exceed 2 V because of various system losses.[12] This increase is primarily due to various energy losses within the system, including activation losses at the electrodes, ohmic losses from resistance in the membrane and other cell components, and concentration losses resulting from mass transport limitations. These inefficiencies necessitate a higher applied voltage to maintain efficient hydrogen production. Specifically prolonged and high current density operations of PEMWE cell produced considerable concentration of protons at the anode side. As a result, the MEA creates a highly acidic and corrosive environment, primarily caused by sulfonic acid functional groups with fluorinated polymer chains.[12–16] Moreover, the highly acidic and oxygen-rich conditions induced by the elevated positive voltage significantly speed up the corrosion

Hydrogen Research Institute, University of Quebec at Trois-Rivières, Trois-Rivières, Québec G8Z 4M3, Canada. E-mail: Samaneh.Shahgaldi@uqtr.ca

and deterioration of metal components such as BPPs and PTLs.[3,14] The PTL is more susceptible to degradation due to its immediate accessibility to the catalyst coated membrane.[17–19] The immediate exposure of PTLs to acidic corrosive environments causes degradation and result in the high ICR through a less conductive passivated layer and the potential to contaminate the catalyst layer, one of the costliest components in a PEMWE cell.[18,20]

Consequently, an exemplary PTL is intended to demonstrate excellent corrosion resistance, high thermal as well as electrical conductivity, and minimal mass transport limitations.[2,9,21–24] The titanium (Ti) based metallic fibers, are prominent for their exceptional resistance to corrosion, are widely employed in the fabrication of different types of PTLs for the application of PEMWEs. However, the Ti PTL passivates when subjected to prolonged high anodic potentials. This process leads to the formation of oxide layers and the gradual breakdown of electron-conductive materials, resulting in increased electrical resistance.[14] In PEMWE systems, precious metals such as Au, Pt and Ir are applied as anti-corrosive coatings on the Ti based PTLs to reduce severe passivation effects on the titanium surface.[20,25,26] This accounts for its significant capital expenditure, despite the method's effectiveness in enhancing electrical conductivity, improving corrosion resistance, and reducing the ICR.[25–27] Kang *et al.* reported that the Ti PTLs electroplated with 180 nm thick Au can decrease the cell voltage to 1.6328 V from 1.6849 V at 2.0 A cm^{-2} and 80 °C temperature.[28] Singh *et al.* explored the engineered electroplating method to deposit an anti-corrosive layer of Au on the Ti-based substrates for PTL applications, and a single-cell performance of 2.0 A cm^{-2} at 1.74 V was demonstrated by utilizing 1 mg cm^{-2} Ir catalyst loading under 80 °C temperature and ambient pressure.[20] Liu *et al.* explored Ir coated Ti PTL by DC sputtering technique for the application of PEMWE.[29] The study identifies degradation effects in PEMWEs due to Ti PTL after 4000 hours of operation and reported that the Ir-sputtered Ti PTL exhibited a stable durability profile achieved with a 0.1 mg cm^{-2} Ir thin layer. Toni *et al.* studied Au, Ir and Pt coatings on the Ti based PTLs as a protective layer and reported that Pt offers high stability initially, but a 10 nm Ir coating provides superior stability for 500 hours of PEMWE operations.[27] As uses of precious metal coatings increase the capital expenditure of PEMWEs, in this aspect, a lot of development has been accomplished to reduce the loading of protective coatings. The pretreatment of the Ti-PTL may serve as a potential approach to reduce the amount of precious metal coating required in the ultra-low loading range. Proper pretreatment to remove TiO_x from Ti-PTL is crucial for strong adhesion of precious metal coatings. The removal of TiO_x layer ensures the uniform nucleation sites for the better adhesion of subsequent coating. Electrochemical etching in acidic media dissolves TiO_x from Ti fibers, promoting TiH_x formation with a more electrically conductive and hydrophilic surface.[30,31] Bautkinova *et al.* reported that the introduction of TiH_x layer on Ti PTL lowers the contact resistance and increase the energy efficiency of PEMWE.[31] Similarly, Stein *et al.* also reported that the TiH_x layer on Ti PTL improves the electrical conduction and reduces degradation rate by 49% overall compared to the uncoated one.[32] Au, a precious metal, has the lowest tendency to oxidize under atmospheric conditions.[33] A thin Au coating on the hydrophilic surface of TiH_x effectively prevents TiO_x formation. The electroplating technique is a straightforward and practical strategy to deposit an Au layer on the PEMWE cell components.[25,28] This well-established electroplating method, being a mature and scalable technology, reduces processing costs and enables low Au loading.[34,35]

Under anodic polarization, Au does not form a persistent, protective oxide layer specifically in acidic environments; as a result, it continuously dissolves into the acidic electrolyte as soluble Au^{3+} ions throughout the prolonged operation.[33] Therefore, a conformal coating of an anticorrosive precious metal on the top of the Au layer is essential for developing a stable Ti-PTL for PEMWE applications in acidic environments. Platinum forms a stable and adherent oxide (like PtO_2) at high potentials, especially in acidic environments. This oxide layer slows down further oxidation (and hence dissolution).

The sputtering technique offers precise control over the deposition process, allowing for uniform and consistent Pt coatings as the top layer at the low loading scale.[36] By accurately controlling the thickness and distribution of the Pt layer, sputtering enhances material efficiency and significantly reduces overall costs, making it a highly attractive method for scalable and cost-effective production of high-performance PTLs. A detailed investigation of low loadings in precious metal-based coatings and comprehensive stability studies under acidic environments is important to produce reliable Ti PTLs for the applications of PEMWE.

As so far conducted studies on Ti PTLs have explored, the single-layer precious metal (Pt, Ir, and Au) coatings modify and surpass the TiO_x passivation, but long-term durability with the low loading of precious metals still is a challenge for the scale-up of cost-effective Ti PTLs. Perhaps there is still a gap in the available literature about the potential of bilayer coatings of Au and Pt to improve the corrosion resistivity, conductivity, and durability with low loading. The interlayer of Au can facilitate high electrical conductivity, and a thin Pt film can ensure the electrochemical stability as well as low ICR of the Ti PTLs. The combination of Au/Pt coating on Ti PTL can surpass the dual challenge of electrical conductivity and high durability with low loading. In this context, this work focuses on a detailed evaluation study of the corrosion and electrochemical performance of Au and Au/Pt coated Ti-PTLs. The comprehensive study was performed using a conventional PEMWE single cell and three-electrode system under PEMWE simulated conditions.

2. Experimental section

2.1. Pre-treatment of Ti PTL substrates

The Ti fiber-based substrates (Bekaert, 68% porosity) with a thickness of 250 μm were selected as PTL for the pretreatment and coating of the precious metals. During the manufacturing process and handling of Ti PTLs, exposure to the ambient environment allowed the natural passivation of TiO_x on the

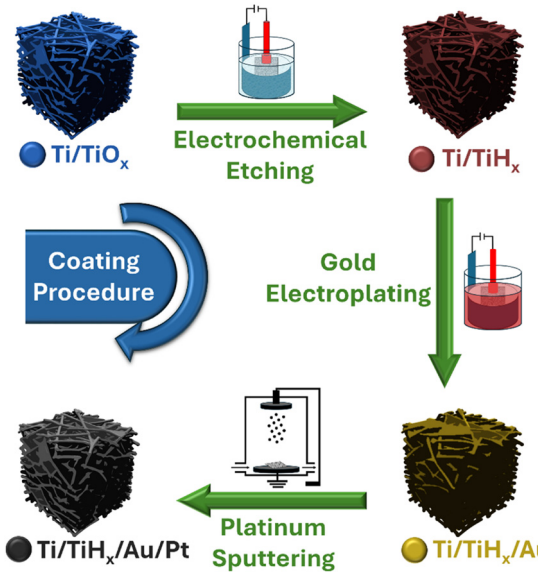

Fig. 1 Schematic diagram of complete treatments of Ti PTLs including Au and Au/Pt bilayer coating.

surface of substrates. Prior to electroplating of Au and deposition of Pt layers, the passivation layer of TiO_x is etched through an electrochemical etching technique, as shown in Fig. 1. Which will further help to enhance the effectiveness of Au electroplating. During the electrochemical etching process, Ti PTL fixed at the cathode electrode holder as a working electrode and a Ti mesh coated with Pt (fuel cell store) were fixed at the anode side as a counter electrode (cylindrical) in an engineered two-electrode system. The Ti PTL was exposed under 0.1 A cm^{-2} current density for 3 min, 6 min, 9 min, and 12 min in a 0.5 M H_2SO_4 acidic electrolyte at 60 °C temperature.

2.2. Au coating on Ti PTLs

An engineered electroplating method was utilized to deposit the Au protective layer on the Ti PTLs. To enhance the exposure of the Au electroplating solution to the porous Ti PTLs, the working electrode (Ti PTL) is rotated at 50 rpm throughout the Au electroplating. The rotation mechanism of Ti PTL not only enhanced the exposure of the Au electroplating solution to the internal arrangements of Ti fibers, but it also made the neutrality of hydrogen bubbles easier throughout the electroplating.[20]

A two-step process is utilized for the coating of the Au layer on Ti PTLs, which includes electro striking and electroplating of Au. In the first step of Au coating, a 24 K acidic Au striking electrolyte (TriVal, Gold Plating Services) was maintained at 22 °C temperature. The etched Ti PTL as a working electrode and cylindrical Ti mesh coated with Pt as a counter electrode are exposed to the Au strike solution under an applied negative potential of 5 V for 30 s. After the 30 s exposure to negative 5 V, the etched Ti PTL surface was nicely adhered and evenly coated with a thin layer of Au that had a little yellow color. During the further electroplating process, this thin electrostriked Au layer offered the highly electrically conductive regions essential for the appropriate coating of the final protective Au layer. Further, during the Au electroplating process, an Au strike Ti PTL was immersed in bright-colored 24 K Au electrolyte (Gold Plating Services) with a similar setup configuration to the Au electro striking. The working electrode (Au strike Ti PTL) was exposed to a negative potential of 3 V for the duration of 300 s at a 40 °C temperature to electroplate the 80 nm Au layer on Ti PTLs.

2.3. Deposition of Pt thin film onto the Au electroplated Ti PTLs

A DC magnetron sputtering technique was utilized to deposit Pt onto the Au coated Ti PTLs, as mentioned in Fig. 1. The Pt thin film was sputtered both sides of the Au coated Ti PTLs using the Pt target (purity: 99.95%). The coating of Pt was conducted on both sides of Au coated Ti PTLs individually, under a base pressure of 1×10^{-5} Torr and a deposition pressure of 3.4×10^{-3} Torr, using Ar gas. The desired loading of the Pt coating was achieved by controlling the deposition time at constant power as shown in Table 1. The sample notations TiH/Au/Pt-0.02, TiH/Au/Pt-0.04, TiH/Au/Pt-0.06, and TiH/Au/Pt-0.08 show loading of 0.02 mg cm^{-2}, 0.04 mg cm^{-2}, 0.06 mg cm^{-2}, and 0.08 mg cm^{-2} of Pt, respectively, on the Au coated Ti PTL substrates. On the other hand, commercially available Pt coated Ti PTL contains almost 0.22 mg cm^{-2} loading.

2.4. Physical characterization

A focused ion beam scanning electron microscope (FIB-SEM; ThermoFisher Helios-5, an accelerating voltage of 20 kV) was used to examine the thickness and elemental composition of Au/Pt bilayer coatings, and the loading of precious metals (Au, and Pt) was analyzed using an X-ray fluorescence spectrometer (XRF; Niton XL2 XRF Analyzer) before and after the corrosion analysis. The X-ray photoelectron spectroscopy (XPS) was utilized to obtain the area percentage of the oxidation state of Au and Pt of the coated PTLs. The XPS was conducted using a Thermo Scientific ESCALab-250 XPS with 150 W Al Ka radiation source ($h\nu$ = 1486.6 eV; monochromatic X-Ray source with an ultimate energy resolution of 0.5 eV). The contact angle measurements were conducted at room temperature after drying the Ti PTLs in vacuum for 2 h at 50 °C. X-ray diffractometer measurements also conducted at room temperature using XRD (Bruker D8 Focus; Source: Cu Kα X-ray tube, λ = 1.5406 Å). For the measurements of contact resistance of the Au coated, and Au/Pt bilayer coated Ti PTLs, ICR measurements were performed under different compressions. A press system (Zwickroel, Germany) of Au-plated copper plates was employed to compress

Table 1 Sputtering parameters for Pt deposition on Au coated Ti PTLs

Sample	Sputtering power (W)	Sputtering time (s)	Pt loading (mg cm^{-2})
TiH/Au/Pt-0.02	120	90	0.02
TiH/Au/Pt-0.04	120	180	0.04
TiH/Au/Pt-0.06	120	270	0.06
TiH/Au/Pt-0.08	120	360	0.08

the Ti PTLs for the ICR measurements. Tests were conducted at room temperature while the samples were compressed in a dry state. The compression that was applied ranged from 0.5 to 5 MPa.

2.5. Electrochemical characterizations

Using potentiodynamic and potentiostatic polarization techniques, the corrosion resistance properties of Au, and Au/Pt bilayer coated Ti PTLs were investigated under 0.5 M H_2SO_4 solution at 80 °C temperature. A conventional corrosion setup was used with a three-electrode configuration, including a working electrode (Ti PTL), reference electrode (saturated Hg/Hg_2SO_4), and counter electrode (platinum wire) and controlled with a Biologic SP-150 potentiostat. The corrosion cell was open to atmosphere and utilized without any further saturation of O_2 or N_2. The working electrode (Ti PTL) with a 1 cm^2 active area was exposed to the 0.5 M H_2SO_4 acidic solution at 2.0 V *vs.* RHE potential to evaluate the corrosion resistance characteristics. The corrosion that Ti based PTLs experienced in a real PEMWE cell could be assessed according to the applied potential range. To assess the stability behavior of corrosion resistance, a 15 h long potentiostatic test was conducted at 2.0 V *vs.* RHE potential.[20,30] Following the potentiodynamic and potentiostatic tests, an electrochemical impedance spectroscopy (EIS) investigation was also performed at OCV, applying the perturbation amplitude of 10 mV and a frequency range of 100 kHz to 0.1 Hz.

The lifetime of the coating was investigated using the galvanostatic method (constant current density of 2.0 A cm^{-2}) in a two-electrode setup under simulated PEMWE conditions. An anode working electrode (Ti PTL) with 1 cm^2 of active area and a cathode counter electrode of a Pt wire were fixed in a 0.5 M H_2SO_4 acidic solution at 80 °C temperature. The duration from the beginning of the experiment and the abrupt rise in voltage to 10 V throughout the galvanostatic test is considered as the coating's overall lifetime.

2.6. *In situ* characterizations

Using a single PEMWE cell unit (Cell-5, Scribner Electrolyzer), the *in situ* characterizations of electrochemical performance of Au, and Au/Pt bilayer coated Ti PTLs were executed. In a single PEMWE cell, a graphite BPP was utilized at the cathode side, whereas Ti BPP with Pt coated single serpentine channels was employed at the anode side. The Coated Ti PTLs (TiH/Au/Pt-0.02, TiH/Au/Pt-0.04, TiH/Au/Pt-0.06, and TiH/Au/Pt-0.08) were used as an anode side PTL, and carbon fiber paper (Fuel Cell Store, thickness 225 μm with MPL) was used as GDL. A commercially purchased 5 cm^2 electrolyzer MEA (Nafion 115; Ion Power) was utilized, with an anode-side catalyst layer of 1.0 mg cm^{-2} Ir and a cathode-side catalyst layer of 0.4 mg cm^{-2} Pt/C. On both the anode and cathode sides, PTFE gaskets with a thickness of 250 μm at the anode and 150 μm at the cathode were utilized for assembling the PEMWE cell. A fully automatic controlled electrolyzer test station (E30; Greenlight Innovation) was used to run the assembled single PEMWE cell to obtain polarization curves and EIS spectra. Only the anodic side of the cell was exposed to the flowing deionized water, which was delivered at a steady 40 mL min^{-1} flow rate at 80 °C. To validate the reproducibility of the results, all the coated Ti PTLs were tested 3 times using the same PEMWE cell under similar operating conditions. Prior to the *I–V* polarization curves and EIS measurements, all cells were conditioned at current densities from 0.2 to 1.0 A cm^{-2} with the increment of 0.2 A cm^{-2} for 30 minutes at every individual current density. Then, by gradually increasing the current density from 0.0 to 4.0 A cm^{-2}, potential was monitored to obtain the *I–V* polarization curves. The galvanostatic EIS spectrums were recorded at different current densities from 0.0 to 2.0 A cm^{-2} with the increment of 0.2 A cm^{-2} at the 100 kHz to 0.1 Hz frequency range and 20% perturbation amplitude. The validation of all measured EIS spectrums confirmed through a Kramers–Kronig test using LIN-KK tool.

3. Results and discussion

3.1. Effect of pre-treatment and surface morphology analysis

The sample etched for 9 min exhibited the lowest contact angle value of 25°, in contrast to 60° for the pristine Ti PTL sample, as shown in Fig. 2(a). The electrochemical etching of the PTLs reduced the contact angle compared to the pristine Ti PTL. The formation of titanium hydride (TiH) during the electrochemical etching on the surface improved the hydrophilic properties of the Ti substrate.[37,38] This enhanced surface wettability of the bare Ti PTL promoted better accessibility to electrochemically active regions throughout the Au electrostriking and electroplating processes.[20] Prolonged electrochemical etching of the Ti PTL for 12 min resulted in a further increase in contact angle to 30° compared to the 9 min etching. Extended cathodic polarization may lead to hydrogen embrittlement, potentially causing surface cracking and exposing areas of the pristine Ti PTL.[39] The ICR analysis was carried out under a range of compression pressures to evaluate the electrical conductivity of the electrochemically etched samples. Fig. 2(b) shows the ICR plots for pristine Ti PTL and samples etched electrochemically for 3, 6, 9, and 12 min. The low contact resistance observed in the etched samples is a result of the development of a conductive TiH_x layer on the Ti PTL.[31,32] The most favorable etching duration was found to be 9 min, yielding the lowest ICR value. However, extending the etching time to 12 minutes resulted in an increase in ICR.

The thickness measurements of Au and Au/Pt bilayers coating were conducted on the top surface of each coated Ti PTL fiber. The thickness of the Au coating was approximately the same, around 80 nm for each sample. The thickness of the Pt was approximately 60 nm, 45 nm, 30 nm, and 15 nm for the Au/Pt 0.08, Au/Pt 0.06, Au/Pt 0.04, and Au/Pt 0.02 samples, respectively (Fig. 3(a–d)). The SEM images in Fig. 3(a–c) confirmed that the surface of the Au coated Ti PTL fiber was uniformly covered with a layer of Pt, while Fig. 3(d) depicts that Pt did not completely cover the Au surface. The SEM images suggest that a minimum Pt coating thickness of

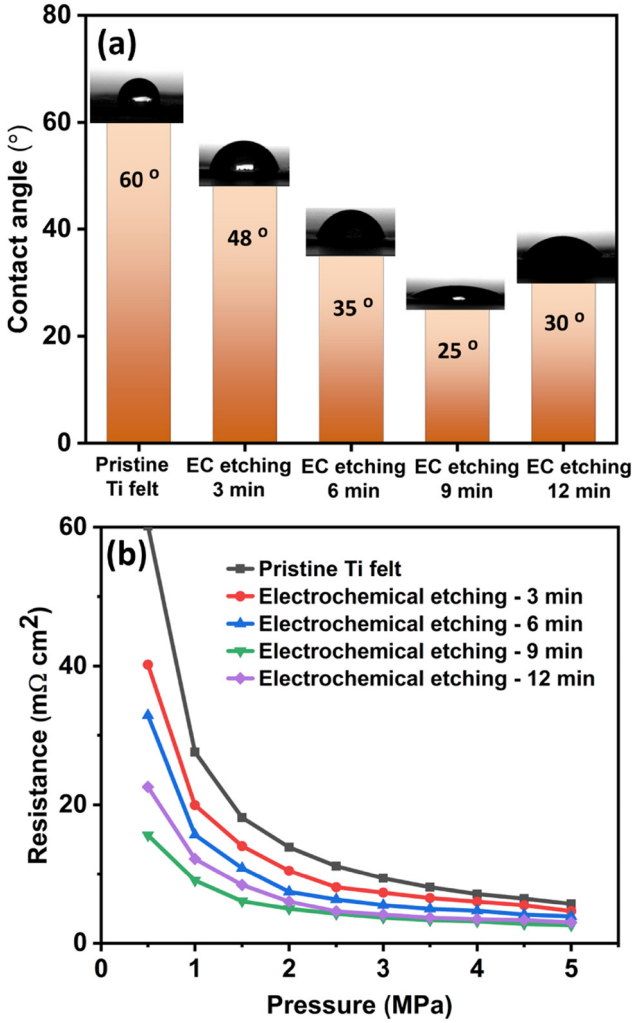

Fig. 2 (a) Contact angle analysis, (b) ICR measurement of pristine Ti PTL and electrochemically etched samples.

30 nm is required to achieve complete coverage of the underlying Au surface. The cross-sectional SEM-EDS analysis of the coated Ti PTLs is provided in the SI in Fig. S1. The quantification of the deposited amount of Au and Au/Pt is not scientifically sensible by utilizing the SEM-EDS technique. Therefore, XRF measurements confirmed each sample's Au loading as 0.08 mg cm^{-2}. The loading of Pt was 0.085 mg cm^{-2}, 0.06 mg cm^{-2}, 0.04 mg cm^{-2}, and 0.02 mg cm^{-2} for the Au/Pt-0.08, Au/Pt-0.06, Au/Pt-0.04, and Au/Pt-0.02 coated Ti PTLs, respectively.

3.2. Corrosion analysis of Au and Au/Pt bilayer coated Ti PTL

In addition to examining the surface morphology and physical characteristics of the Au coated Ti PTL and the Au/Pt bilayer coatings on Ti PTLs, it is essential to investigate the specific role of the Pt coating on the surface of the Au coated Ti PTL. In this work, corrosion analysis was conducted using simulated PEMWE conditions, including 0.5 M H_2SO_4 solution at 80 °C temperature. The potentiodynamic and Potentiostatic studies were performed to examine the effect of sputtered Pt thin layer onto the Au coated Ti PTLs. As mentioned in Fig. 4(a), the corrosion current density of the Au coated Ti PTL (TiH/Au), TiH/Au/Pt-0.02, TiH/Au/Pt-0.04, TiH/Au/Pt-0.06, and TiH/Au/Pt-0.08 PTL samples is 0.11 μA cm^{-2}, 0.098 μA cm^{-2}, 0.085 μA cm^{-2}, 0.065 μA cm^{-2}, and 0.066 μA cm^{-2}, respectively. The corrosion current density of TiH/Au/Pt-0.06 is 1.7 times, 1.5 times, and 1.3 times lower than that of the counterparts TiH/Au, TiH/Au/Pt-0.02, and TiH/Au/Pt-0.04, respectively. The potentiodynamic polarization curve showed similar corrosion current densities of TiH/Au/Pt-0.06 and TiH/Au/Pt-0.08 PTL samples, because beyond the critical thickness, adding more Pt doesn't significantly enhance protection, so the corrosion current remains unchanged. On the other hand, the observed downward peak in Fig. 4(a), which corresponds to the corrosion potential, is also consistent with the findings of corrosion current densities in the case of the bilayer coating of Au/Pt. The TiH/Au/Pt-0.06 and TiH/Au/Pt-0.08 PTL samples demonstrated more positive corrosion potential than the TiH/Au, TiH/Au/Pt-0.02 and TiH/Au/Pt-0.04 samples. A thin top layer of Pt with high corrosion potential might also form a stable passive layer that resists breakdown. This passivity leads to long-term corrosion resistance, even in harsh acidic media.[40] The performed potentiodynamic test exhibited that the Au/Pt bilayer coated Ti PTL demonstrated an excellent corrosion resistance characteristic at the applied potential range under acidic environmental conditions. As compared to the only Au coated PTL sample, this excellent corrosion resistance may be accountable for the exceptional stability of Au/Pt bilayer coated Ti PTLs and further enhanced the restoration of passivation characteristic through Au/Pt bilayer coatings; similarly, other authors have also indicated.[41]

In Fig. 4(b), TiH/Au, TiH/Au/Pt-0.02, TiH/Au/Pt-0.04, TiH/Au/Pt-0.06, and TiH/Au/Pt-0.08 coated Ti PTL showed an OCV of 0.41 V, 0.63 V, 0.74 V, 0.79 V, and 0.81 V *vs.* RHE, respectively. The TiH/Au/Pt-0.06, and TiH/Au/Pt-0.08 samples demonstrated high positive values of OCV than TiH/Au, TiH/Au/Pt-0.02, TiH/Au/Pt-0.04 samples. This indicates that the uniform coating of Pt is highly vulnerable to passivation under an acidic environment, while it releases at most a minimal number of sacrificial electrons.[42,43] In comparison to Au, the Pt exhibited high OCV values because Pt has a greater work function than Au.[44] As a result, Pt resists electron loss (oxidation), and it stabilizes the electrode at a greater positive potential.[9,23,45]

Furthermore, the anti-corrosive properties of the only Au coated, and Au/Pt bilayer coated Ti PTLs were investigated at OCV utilizing the EIS technique. As mentioned in Fig. 4(c), the R_{CT} denotes the charge transfer resistance between the coated Ti PTLs and the acidic solution, C_{DL} denotes the double layer capacitance, and R_S stands for the resistance of the acidic solution.[20,23,30,45] The surface coating's inhomogeneity is the cause of the constant phase element (CPE), while in addition the Au/Pt bilayer coated Ti PTL's anti-corrosive coating is responsible for the added corrosion resistance (R_{ACR}). The Nyquist plots of Au/Pt bilayer coated Ti PTL exhibited greater semicircle diameter than those of TiH/Au in simulated PEMWE conditions; it shows that higher corrosion resistance (R_{ACR})

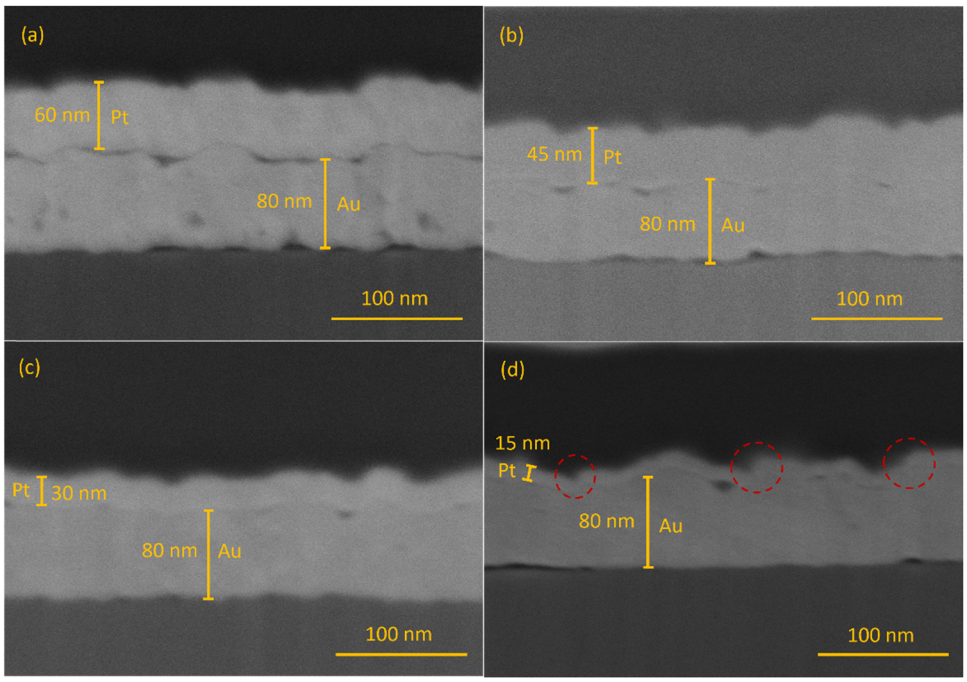

Fig. 3 Cross-sectional SEM images obtained from FIB-SEM of (a) TiH/Au/Pt-0.08, (b) TiH/Au/Pt-0.06, (c) TiH/Au/Pt-0.04, and (d) TiH/Au/Pt-0.02 coated Ti PTLs.

improves the charge transfer resistance at OCV in between the Au/Pt bilayer coated Ti PTL and 0.5 M H_2SO_4 solution.[42,43] Table 2 contains the values of R_{CT}, R_S, and R_{ACR} obtained from the equivalent circuits of EIS (fitted EIS plot and parameters are provided in SI Fig. S2 and Table S1). The TiH/Au/Pt-0.06 coated Ti PTL presented the lowest value of R_S, which is due to the conformal coating of a highly conductive Pt layer on the Au coated Ti PTL, resulting in high electron transfer. In the case of TiH/Au/Pt-0.06 coated Ti PTL, the R_{CT} value is higher than that of TiH/Au, TiH/Au/Pt-0.02, TiH/Au/Pt-0.04, and TiH/Au/Pt-0.08 coated Ti PTLs, which indicates that the thin layer of Pt with 0.06 mg cm^{-2} loading on the Au coated Ti PTL exhibits superior corrosion resistance. The noble and anti-corrosive nature of Au/Pt bilayer coating led to the observation of the function of an extra charge transfer resistance (R_{ACR}). The highest value of R_{ACR} regarding the TiH/Au/Pt-0.06 coated Ti PTL indicates that sputtered Pt coating on the Au coated Ti PTL can enhance the anti-corrosion properties of the protective film. This protective film effectively blocks the penetration of aggressive ions (like H^+) from reaching and attacking the underlying Au or Ti fibre. The results obtained from the Nyquist plot agree with potentiodynamic polarization analysis.

Based on the potentiostatic polarization curves at 2.0 V *vs.* RHE, the current density of the Au coated Ti PTL decreases quickly within the first 30 to 40 minutes, as shown in Fig. 4(d). This abrupt reduction in current density might be caused by electrochemical cleaning of the coated Ti PTL surface and erosion of the oxide layer due to the generated oxygen bubbles. Subsequently, the increase in potentiostatic current was observed, possibly due to the nucleation of the gold oxide (Au^{3+}) under positive applied potential.[46] In addition, the TiH/Au/Pt-0.02 and TiH/Au/Pt-0.04 Ti PTL samples show an exponential decay in the current at applied potential. The exponential decrease might be due to the gold oxide (Au^{3+}) layer dissolution in acidic electrolyte.[33,47] Regarding the TiH/Au/Pt-0.06 coated Ti PTL, the current density at potentiostatic polarization reduced rapidly, obtaining the steady-state and lowest current density. It is observed that the nominal thickness of Pt on the Au coated sample shows better stability. This is often due to forming a stable passive film that protects the underlying metal in acidic solution. Therefore, forming a stable bilayer of Au/Pt-0.06 could notably boost the corrosion resistance of the Ti PTL.

3.3. The ICR measurement before and after potentiostatic test

The ICR measurements were performed under different compression pressures to investigate the electrical conductivity of the Au and Au/Pt bilayer coated Ti PTL samples. Fig. 5(a) depicts the ICR values of TiH/Au, TiH/Au/Pt-0.02, TiH/Au/Pt-0.04, TiH/Au/Pt-0.06, and TiH/Au/Pt-0.08 PTL samples both prior and after the potentiostatic test for 15 h. The low ICR values of each sample were attributed to an electrically conductive, conformal coating on Ti PTLs. The fresh samples did not show a significant difference in ICR values due to an identical conductive coating (Au, Pt) on Ti PTLs. The Au/Pt bilayer coated Ti PTL demonstrated a low ICR of 5 mΩ cm^2 at a compression of 1.5 MPa. The Au coated Ti PTL presented a slightly higher ICR value within the compression range between 0.5 and 2.0 MPa. The decreased ICR of Au/Pt coated Ti PTLs is attributed to forming a compatible bilayer system; the interface between them can help reduce electron scattering.[7,9,23]

Although the Au/Pt coated Ti PTL significantly reduced the ICR, maintaining low contact resistance after the potentiostatic

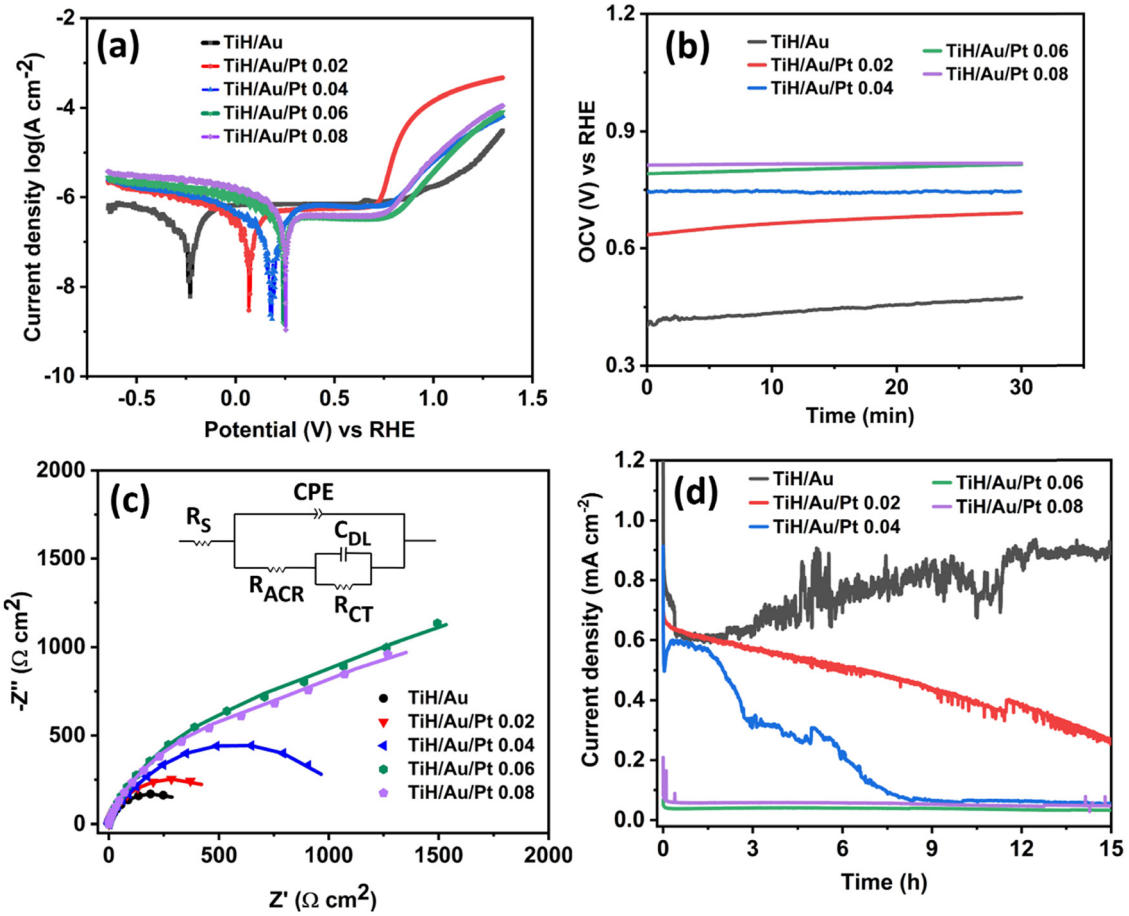

Fig. 4 (a) Potentiodynamic polarization curve (b) open circuit voltage (OCV) (c) EIS at OCV (d) potentiostatic polarization for 15 h at 2.0 V *vs.* RHE of the TiH/Au, TiH/Au/Pt-0.02, TiH/Au/Pt-0.04, TiH/Au/Pt-0.06, and TiH/Au/Pt-0.08 PTL samples.

Table 2 Values obtained from the fitted equivalent circuit model

Samples	R_S (Ω cm^2)	R_{CT} (Ω cm^2)	R_{ACR} (Ω cm^2)
TiH/Au	1.38	490	—
TiH/Au/Pt-0.02	1.42	620	45
TiH/Au/Pt-0.04	1.4	1100	120
TiH/Au/Pt-0.06	1.25	4200	1500
TiH/Au/Pt-0.08	1.1	4100	1250

test in acidic media remains the primary challenge. Even with the potentiostatic test, the ICR values of the TiH/Au/Pt-0.06 sample remained as low as 9.1 mΩ cm^2. The TiH/Au, TiH/Au/Pt-0.02, TiH/Au/Pt-0.04, and TiH/Au/Pt-0.08 coated Ti PTLs exhibited significantly high ICR values of 27 mΩ cm^2, 19 mΩ cm^2, 12 mΩ cm^2, and 10.7 mΩ cm^2 at 1.5 MPa, respectively. In conclusion, the conformal coating of the Pt thin layer on the Au coated Ti fiber effectively prevented the gold's dissolution. Moreover, the ICR results are consistent with the observation of potentiodynamic and potentiostatic tests during corrosion analysis.

In Fig. 5(b), the XRD analysis of the Au coated Ti PTLs exhibited diffraction peaks associated with (311), (220), (200), and (111) at 2θ angles of 77.5°, 64.7°, 44.2°, and 38°. The diffraction peaks corresponding of the Au crystal structure are consistent with JCPDS file number [04-0784].[48] The TiH/Au/Pt-0.06 coated Ti PTL showed precise additional peaks at 46° and 67.6° 2θ angles, referred to as Pt (200) and Pt (220) planes, respectively (JCPDS file number [04-0346]). In the case of TiH_x/Au sample, after the potentiostatic test, the intensity of peaks corresponding to Au has decreased, possibly due to the Au dissolution in acidic electrolyte under positive applied potential. The Au layer's detachment from the Ti PTL increases ohmic and mass transfer resistance in the PEMWE.[12,15] In addition, after the potentiostatic test, the Au coated Ti PTL showed diffraction peaks at angles of 25.8° and 49.1°, corresponding to TiO_2, which may be attributed to the oxidation of the Ti PTL substrate at exposed sites on the Au coated Ti PTL. The TiH/Au/Pt-0.06 coated Ti PTL showed negligible change in the diffraction pattern after the potentiostatic test. The top layer coating of Pt on the Au coated Ti PTL showed a strong anti-corrosion property in acidic media under positive applied potential.

Importantly, XPS analysis (Fig. 5c and d) revealed that the oxidation states of Au and Pt after the potentiostatic tests were significantly influenced by the most favorable Pt coating on the Au coated Ti PTL. The proportion of metallic Au^0 content

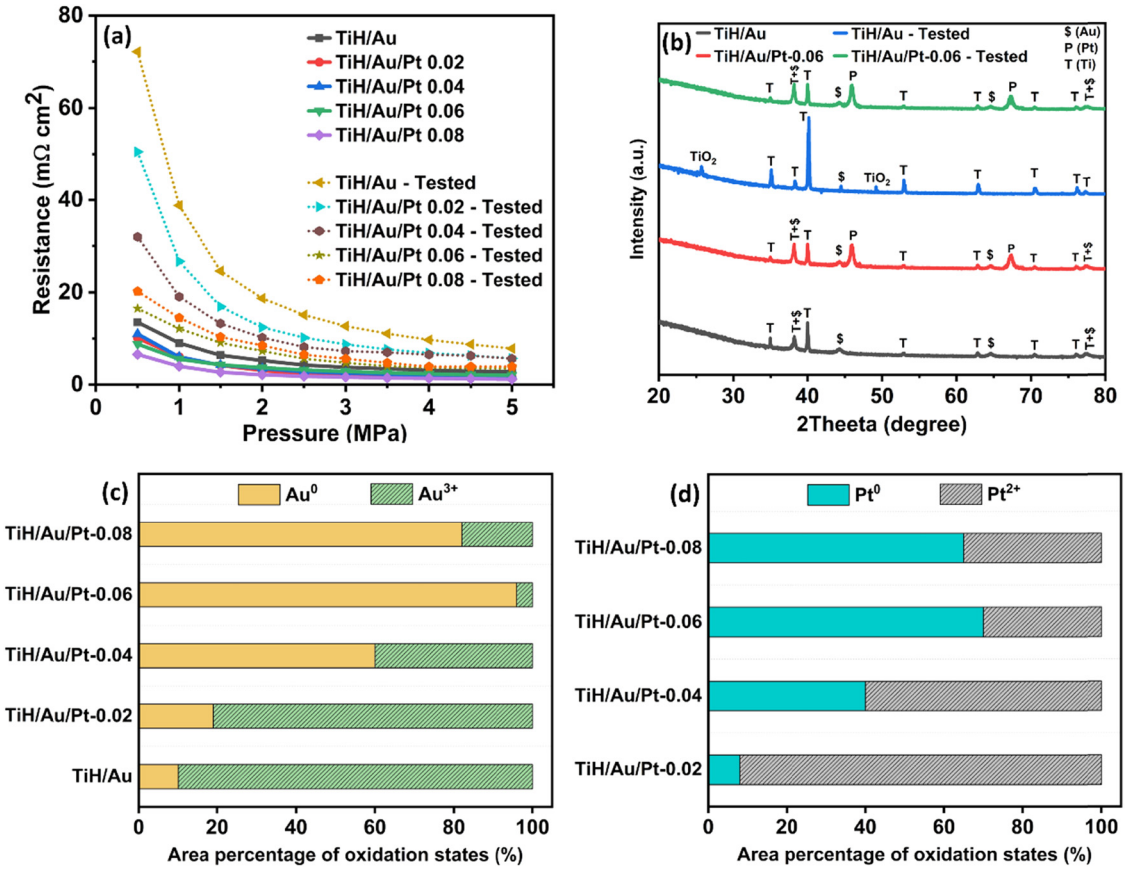

Fig. 5 (a) ICR plots of TiH/Au, TiH/Au/Pt-0.02, TiH/Au/Pt-0.04, TiH/Au/Pt-0.06, and TiH/Au/Pt-0.08 coated Ti PTL before and after the potentiostatic test, (b) XRD spectra of TiH/Au and TiH/Au/Pt-0.06 before and after the potentiostatic test, (c) and (d) XPS-derived area percentage of oxidation state of TiH/Au, TiH/Au/Pt-0.02, TiH/Au/Pt-0.04, TiH/Au/Pt-0.06, and TiH/Au/Pt-0.08 coated Ti PTL after the potentiostatic test.

decreased to 10% in the Au coated Ti PTL (TiH/Au), whereas it increased to 90% in the case of low Pt loading of 0.06 mg cm^{-2} (TiH/Au/Pt-0.06). Similarly, the Pt film exhibited a less oxidized state in the optimally coated TiH/Au/Pt-0.06 sample, with the proportion of metallic Pt^0 reaching 75%. In contrast, the TiH/Au/Pt-0.02, TiH/Au/Pt-0.04, and TiH/Au/Pt-0.08 samples showed lower metallic Pt^0 contents of 8%, 40%, and 69%, respectively. This trend was further supported by lifetime analysis, which quantified the remaining metallic Pt and Au on the bilayer coating. The results of the XRD and XPS analyses indicate that the most favorable Pt loading of 0.06 mg cm^{-2} on the Au coated Ti PTL effectively reduced the oxidation states of both Au and Pt under potentiostatic testing conditions. Evidently, the reduced oxidation state of Au was vital for retaining the structural integrity of the top Pt coating. Although the presence of Pt^{2+} contributes to the stability of the top layer, the presence of metallic Pt is also essential for maintaining the desirable electrical conductivity of the film, as supported by the ICR results of the coated Ti PTL after the potentiostatic tests.

3.4. *Ex situ* lifetime testing of the Au and Au/Pt bilayer coated Ti PTLs

The lifetime of the coating is investigated using the galvanostatic method in a two-electrode setup including an anode working electrode (Ti PTL) with 1 cm^2 of active area and a cathode counter electrode of a Pt wire. The duration from the beginning of the measurement and the abrupt rise in voltage to 10 V throughout the experiment is considered as the coating's overall lifetime.[18,23,24,32] The rapid increase in voltage is due to the oxidation and dissolution of the Au and Au/Pt metal coating under the applied current.[9,23,49] Fig. 6(a) contains information on the *ex situ* lifetime of the coatings. At identical testing conditions, the coating of TiH/Au/Pt-0.06 exhibited 23 times, 3.5 times, 1.6 times, and 1.2 times improved *ex situ* lifetime compared to the TiH/Au, TiH/Au/Pt-0.02, TiH/Au/Pt-0.04, and TiH/Au/Pt-0.08, respectively. In the case of TiH/Au/Pt-0.02 and TiH/Au/Pt-0.04 coated Ti PTL, the interlayer Au is not adequately covered with Pt. Under a positive potential, Au metal oxidizes, forming metal ions (Au^{3+}) that dissolve into the acidic solution. The TiH/Au/Pt-0.08 coated Ti PTL showed poor lifetime as compared to TiH/Au/Pt-0.06, due to the presence of a thick Pt layer on the surface of the Au coated Ti PTL. The thick Pt layer may cause excessive residual shear stress at the Au–Pt interface, leading to poor adhesion between the Pt and Au layers.[50,51]

It is assumed that the durability of coated Ti PTLs is significantly affected by the dissolution of coating layers, such as Au and Pt.[20] An oxidative environment created by an applied

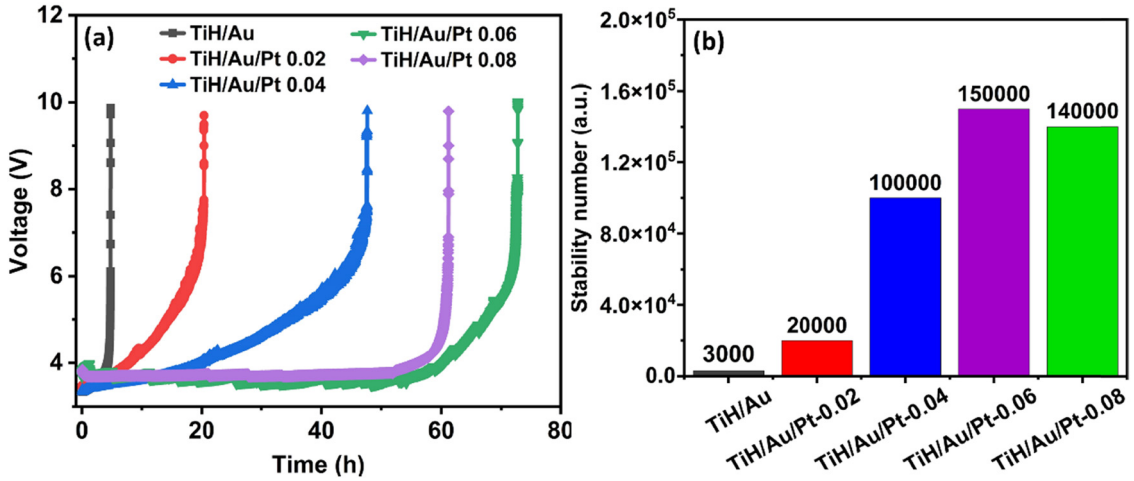

Fig. 6 (a) Full lifetime test, (b) stability numbers of TiH/Au, TiH/Au/Pt-0.02, TiH/Au/Pt-0.04, TiH/Au/Pt-0.06, and TiH/Au/Pt-0.08 coated Ti PTL.

current generates oxygen at the coated Ti PTL. As the coating dissolves, the exposed Ti PTL becomes more susceptible to corrosion, increasing ICR and reducing energy efficiency, which makes it harder to drive the oxygen evolution reaction (OER). The quantity of precious metals dissolved from the protective layer of Ti PTLs is expressed relative to the amount of evolved oxygen, forming a self-sustaining metric known as the stability number as mentioned in SI.[30,52,53] Geiger *et al.* utilized concept of the stability numbers to assess the dissolution behavior of OER electrocatalysts in acidic environments, including the Ir metal from Sr_2PrIrO_6, $SrIrO_3$, and amorphous and crystalline IrO_x.[53] Fundamentally, the stability number facilitates direct evaluation of coating lifespan, allows for rapid comparison of durability, and provides the information on the degradation mechanisms under specific operating conditions.[30,52,53] The stability number of the Au and Au/Pt bilayer coated Ti PTLs is calculated under the same acidic conditions to validate the *ex situ* durability results. The TiH/Au/Pt-0.06 (1.5×10^5) coated Ti PTL showed a higher stability number than the stability numbers of TiH/Au (3.0×10^3), TiH/Au/Pt-0.02 (2.0×10^4), TiH/Au/Pt-0.04 (1.0×10^5), and TiH/Au/Pt-0.08 (1.4×10^5) coated Ti PTL, as shown in Fig. 6(b). The high stability number of TiH/Au/Pt-0.06 indicates that the coated titanium PTL can withstand an oxidative environment with minimal dissolution of Au/Pt coating.

3.5. *In situ* performance evaluation of Au and Au/Pt bilayer coated Ti PTL

The Au, and Au/Pt bilayer coated Ti PTLs were analysed for their durability in acidic environments (0.5 M H_2SO_4) through corrosion testing, as well as in long-term trials using a controlled two-electrode simulation setup. In addition to isolated performance testing, it is essential to understand how these coated PTLs behave under realistic operating conditions, including variations in applied pressure, temperature, and interactions with electrolytes. Real-time cell testing provides valuable insights into the operational behavior of the coated PTLs and enables evaluation of their performance when integrated with other electrolyzer components, such as the membrane electrode assembly (MEA) and bipolar plates. This comprehensive approach helps confirm the coating's reliability in a fully operational system. The *I–V* pol-curves for Au coated (TiH/Au) and bilayer (TiH/Au/Pt) coated Ti PTLs were recorded using a PEMWE single cell. The protective layer coating was applied to the same Ti PTL substrate; therefore, the pore structure of the aforementioned PTLs is nearly identical. The coating thickness ranges from 80 to 140 nm, while the average pore size of the Ti-PTL is approximately 20 μm. Due to the significant difference between coating thickness and pore size, each coated PTL exhibits similar mass transport losses.

In Fig. 7(a), the TiH/Au/Pt-0.06 coated Ti PTL exhibited better single cell performance than TiH/Au, TiH/Au/Pt-0.02, and TiH/Au/Pt-0.04 coated Ti PTLs. The *I–V* polarization curves strengthen the superior electrical conductivity of TiH/Au/Pt-0.06 coated Ti PTL as a result of excellent interfacial contact between Au and the Pt layer. The most favorable low Pt loading of 0.06 mg cm^{-2} on Au coated Ti PTL balances stress between the Au and Pt layers while potentially reducing the cell voltage in a PEMWE single cell. The balanced stress at the Au/Pt interface offered the accelerated electron transfer from Pt to Au.[51] The TiH/Au/Pt-0.06 coated Ti PTL exhibited enhanced PEMWE single cell performance of 1.716 V at a current density of 2.0 A cm^{-2}, which is exceeding those reported in open studies.[7,21,49,54–57] The high ohmic resistances of the TiH/Au TiH/Au/Pt-0.02, and TiH/Au/Pt-0.04 coated Ti PTLs elevated the potential to 1.826 V, 1.792 V, and 1.778 V, respectively, at 2.0 A cm^{-2}. The TiH/Au/Pt-0.02 and TiH/Au/Pt-0.04 coated Ti PTLs contain ultra-low loadings of Pt, may not be sufficient to cover the Au coating uniformly. The inhomogeneity of the Pt coating resulted in a localized area that does not facilitate efficient electron transfer. The TiH/Au/Pt-0.06 and TiH/Au/Pt-0.08 coated Ti PTL have shown nearly identical performance. Similar performance indicates that Pt loadings above 0.06 mg cm^{-2} do not contribute to a further reduction in ohmic resistance at the PTL/CL interface. Although the TiH/Au/Pt-0.06 and TiH/Au/Pt-0.08 coated Ti PTLs exhibited similar performance in a single

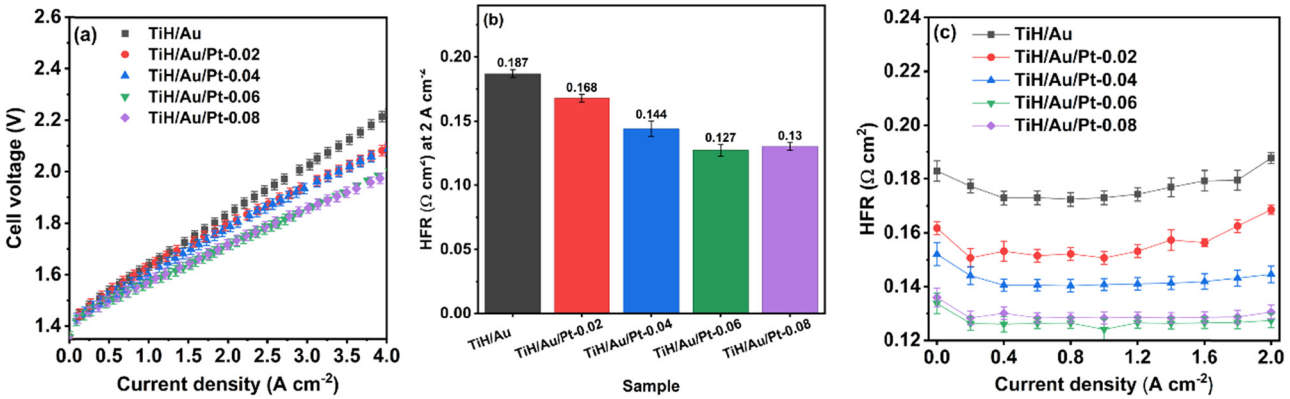

Fig. 7 (a) Polarization curve, and (b) HFR at 2.0 A cm^{-2} current density, (c) HFR values at different current densities.

cell, the TiH/Au/Pt-0.06 demonstrated superior long-term durability in acidic media under simulated operating conditions. The PEMWE single cell performance of coated Ti PTLs was consistent with ICR results and the electrochemical corrosion study.

The most favorable loading of Pt on the Au coated Ti PTL offered strong contact at the CL/PTL interface, improving kinetics and reducing the value of high-frequency resistance (HFR). Generally, the HFR comprises both the membrane resistance and the electrical contact resistance.[7,29] In this work, the resistance associated with the membrane is identical in the case of all five assembled cells, due to the use of similar MEA. The protective layer of bilayer coating has increased the electrically conductive sites in contact with the CL while minimizing the degradation of catalyst under compression.[27,29] The best TiH/Au/Pt-0.06 coated Ti PTL enabled an improved catalyst utilization as compared to other PTL counterparts. As shown in Fig. 7(b), the HFR values of TiH/Au/Pt-0.06 and TiH/Au/Pt-0.08 coated PTLs were lowest and remained constant, while HFR values of TiH/Au, TiH/Au/Pt-0.02, and TiH/Au/Pt-0.04 coated Ti PTL samples were high at similar current densities. The EIS measurements at different current densities (low, medium, and high) can provide insightful information about enhanced PEMWE cell performance using bilayer coated Ti PTLs. In Fig. 7(c), the HFR *vs.* current density curve was derived by the galvanostatic EIS study performed at different current densities from 0.0 to 2.0 A cm^{-2}. In the initial measurements at 0.0 to 0.2 A cm^{-2} current densities, the HFR values were slightly decreases in the case of all samples, this is a typical phenomenon which is related to the heating, and hydration of PEM results in the high proton conductivity.[23,58–60] The PEM, which is mainly responsible for H^+ conduction between the anode and cathode side of the cell, contains an inherent proton transport resistance. As PEM is a solid electrolyte of PEMWE cell, this resistance can be referred to as electrolyte ohmic resistance. At very low current densities (0.0–0.1 A cm^{-2}), the rate of H^+ formation is relatively lower than high current densities, resulting in an insignificant osmotic drag of water throughout the PEM, and slightly high HFR. In the case of increased current density to 0.2 A cm^{-2} due to significant hydration of PEM, results in lower HFR values.[20,61,62] On the other hand increase in the HFR values of TiH/Au and TiH/Au/Pt-0.02 coated Ti PTLs, can be related to the non-uniformly coated Ti fibers and exposed Ti surface which causes the baubles accumulation results in high HFR values after the 1.2 A cm^{-2} current density.

As shown in Fig. 8(a), in the case of EIS at low current density (0.2 A cm^{-2}), TiH/Au sample exhibited highest dimeter of the semi-circle, compared to the TiH/Au/Pt coated samples. Which is clearly sign of poor conductive interface between PTL/CL, and less catalyst utilization results in low OER activity. On the other hand, while increasing the Pt loading at TiH/Au coated Ti PTLs, results in high catalyst utilization, specifically for OER activity at low current density (0.2 A cm^{-2}) where mass transport losses are considered negligible. As shown in Fig. 8(b), in the case of medium current density (1.0 A cm^{-2}), the addition of second semi-circle at low frequency range attributes to minor mass transport losses, as well as at high current density also (2.0 A cm^{-2}) these losses are lower and identical shown in Fig. 8(c). Which is a clear sign of negligible porosity alteration during the electroplating of Au and sputtering of Pt with different loadings. Furthermore, Kramers–Kronig test was also conducted using LIN-KK tool to validate the linearity and stability of all measured EIS spectrums. The residuals of all spectrums were in the range of 0.2 to 0.3% which is considered normal.[63,64] All the residual and Nyquist plots are provided in the SI Fig. S3–S5.

Although a high loading of Au/Pt bilayer on PTLs may significantly reduce the HFR, it can also result in poor adhesion and increased production costs. A platinum loading above 0.06 mg cm^{-2} may result in low HFR, but it can also lead to poor stability of the coated PTLs during long-term operation. The limited durability of PTLs with high Pt loading (0.08 mg cm^{-2}) has been observed in the previously discussed chronoamperometry, lifetime, and stability number analyses. It can be concluded that the most favourable TiH/Au/Pt-0.06 coating on the Ti PTL substrate significantly enhances electrical contact at the CL/PTL interface. In-terms of durability analysis, TiH/Au/Pt-0.06 sample were tested for prolonged is-situ operation at 2.0 A cm^{-2} current density under similar operating conditions for 217 h. As shown in SI Fig. S6, TiH/Au/Pt-0.06 sample exhibited superior durability

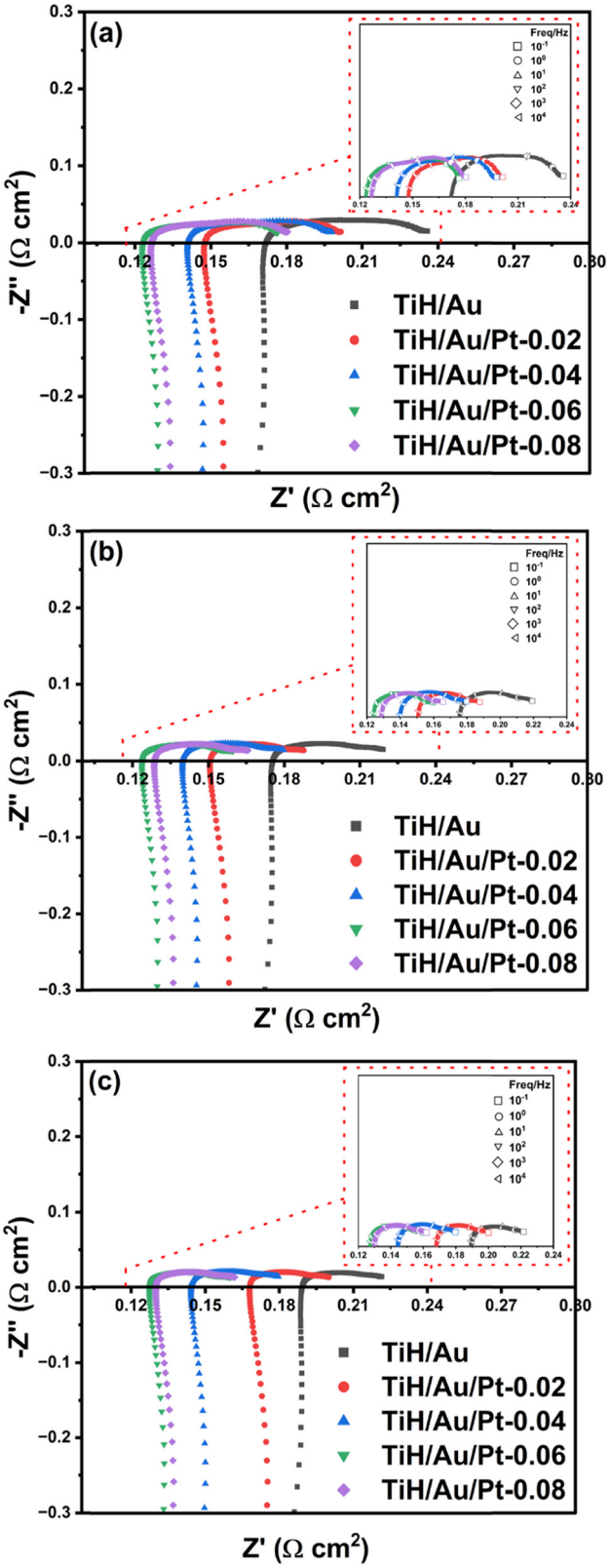

Fig. 8 (a) EIS at 0.2 A cm^{-2} current density (b) EIS at 1.0 A cm^{-2} current density, and (c) EIS at 2.0 A cm^{-2} current density plots of TiH/Au, TiH/Au/Pt-0.02, TiH/Au/Pt-0.04, TiH/Au/Pt-0.06, and TiH/Au/Pt-0.08 coated Ti PTL.

then TiH/Au coated Ti PTL. The degradation rate was 7.1 μV h^{-1} observed in the case of TiH/Au/Pt-0.06, which is 11.4 times lower compared to TiH/Au sample. Surprisingly, degradation rate of TiH/Au sample reached 81.4 μV h^{-1} in just 70 h *in situ* operation. On the other hand, one common tread is observed in both samples, cell performance was slightly increased in initial 15 h, which can be primarily referred to the conditioning or activation of the MEA.[65] This approach demonstrates strong potential for improving performance of PEMWE and owing to the ability to utilize low loadings of precious metals.

The Au/Pt bilayer coating on the Ti PTL substrate exhibited superior electrochemical performance for the PEMWE systems. Its corrosion-resistant characteristics effectively shielded the Ti fibers from deterioration in acidic environments, while the synergy between Au and Pt layers presents a viable route to minimize the use of expensive precious metals. This method decreases dependence on high-cost materials, enhancing the economic feasibility of PEMWE technology. The outlined approach supports major progress toward scalable and affordable hydrogen generation, positioning PEMWEs as essential elements in the transition to sustainable energy infrastructure.

4. Conclusions

Herein, a bilayer coating of Au/Pt was applied to control the degradation of Ti felt-based PTLs for the application of PEMWE. The sputtered Pt top layer effectively suppressed the dissolution of the electroplated Au underlayer in an acidic environment (0.5 M H_2SO_4). The bilayer coating effectively reduced the loadings of Au and Pt to a low level (overall 0.14 mg cm^{-2}) but also exhibited excellent anti-corrosion characteristics under simulated PEMWE conditions. The most favorable loading of Pt of 0.06 mg cm^{-2} on the Au coated Ti PTL presented an enhanced charge transfer resistance. The stability number as a metric was utilized to quickly compare the robustness of various coatings, allowing for a straightforward assessment of their longevity under applied current. The TiH/Au/Pt-0.06 bilayer coated Ti PTL showed a stability number that was 50, 7.5, 1.5, and 1.1 times higher than the stability number of the TiH/Au, TiH/Au/Pt-0.02, TiH/Au/Pt-0.04, and TiH/Au/Pt-0.08 samples. In the case of 0.08 mg cm^{-2} loading of Pt effectively reduced the adhesion on the Au coated Ti PTL, causing limited stability during long-term operation and significantly increasing production costs. The TiH/Au/Pt-0.06 coated Ti PTL showed high PEMWE performance of 1.716 V at 2.0 A cm^{-2}, employing a commercial MEA with 1 mg cm^{-2} Ir catalyst. The Au/Pt bilayer coating enhanced the high electrically conductive sites at the PTL/CL interface, owing to the efficient utilization of the catalyst. The Au/Pt bilayer coated Ti PTL showed excellent stability, demonstrating the potential of bilayer coatings for increasing the performance as well as scalability of PEMWE applications.

Author contributions

Sukhvant Singh – writing (original draft), formal analysis, investigation, methodology, visualization. Aditya Singh – investigation,

validation, writing (review and editing). Muhammad Azhar Iqbal – data curation, investigation, formal analysis, and validation. Samaneh Shahgaldi – project administration, resources, supervision, validation, review and editing.

Conflicts of interest

All authors have no conflicts of interest.

Data availability

The reported data in this research article is completely generated by the authors and stored in research group facilities (dedicated laboratory space provided by UQTR Canada). All electrochemical data including polarization curves, OCV, EIS, Tafel plot, durability test and physical characterization data including SEM, XRD completely mentioned in the article and will be available from the authors upon the reasonable request.

The data supporting this article have been included as part of the supplementary information (SI). Supplementary information is available. See DOI: https://doi.org/10.1039/d5ya00274e.

Acknowledgements

This project was financially supported by Mitacs Accelerate (Application Ref.: IT29926) in collaboration with Intlvac Thin Film. The authors gratefully acknowledge additional funding from the Natural Sciences and Engineering Research Council of Canada (NSERC) through the Canada Research Chair (CRC-2019-00354) and Discovery Grant (CRSNG-DGECR-2022-00058). The technical assistance provided by the Intlvac team is also sincerely appreciated.

References

1 L. Li, P. Wang, Q. Shao and X. Huang, Recent Progress in Advanced Electrocatalyst Design for Acidic Oxygen Evolution Reaction, *Adv. Mater.*, 2021, **33**(50), 1–24. Available from: https://advanced.onlinelibrary.wiley.com/doi/10.1002/adma.202004243.

2 X. Z. Yuan, N. Shaigan, C. Song, M. Aujla, V. Neburchilov and J. T. H. Kwan, *et al.*, The porous transport layer in proton exchange membrane water electrolysis: perspectives on a complex component, *Sustainable Energy Fuels*, 2022, **6**(8), 1824–1853. Available from: https://xlink.rsc.org/?DOI=D2SE00260D.

3 T. Wilberforce, O. Ijaodola, E. Ogungbemi, F. N. Khatib, T. Leslie and Z. El-Hassan, *et al.*, Technical evaluation of proton exchange membrane (PEM) fuel cell performance – A review of the effects of bipolar plates coating, *Renewable Sustainable Energy Rev.*, 2019, **113**, 109286. Available from: https://doi.org/10.1016/j.rser.2019.109286.

4 C. Hu, Y. Hu, B. Zhang, H. Zhang, X. Bao and J. Zhang, *et al.*, Advanced Catalyst Design Strategies and In-Situ Characterization Techniques for Enhancing Electrocatalytic Activity and Stability of Oxygen Evolution Reaction, *Electrochem. Energy Rev.*, 2024, **7**(1), 19. Available from: https://doi.org/10.1007/s41918-024-00219-8.

5 M. Wu, F. Dong, Y. Yang, X. Cui, X. Liu and Y. Zhu, *et al.*, Emerging Atomically Precise Metal Nanoclusters and Ultrasmall Nanoparticles for Efficient Electrochemical Energy Catalysis: Synthesis Strategies and Surface/Interface Engineering, *Electrochem. Energy Rev.*, 2024, **7**(1), 10. Available from: https://link.springer.com/10.1007/s41918-024-00217-w.

6 G. Liu, S. Liu, X. Li, H. Lv, H. Qu and Q. Quan, *et al.*, Optimized W-d band configuration in porous sodium tungsten bronze octahedron enabling Pt-like and wide-pH hydrogen evolution, *Nano Energy*, 2024, **123**, 109442. Available from: https://linkinghub.elsevier.com/retrieve/pii/S2211285524001903.

7 C. Liu, K. Wippermann, M. Rasinski, Y. Suo, M. Shviro and M. Carmo, *et al.*, Constructing a Multifunctional Interface between Membrane and Porous Transport Layer for Water Electrolyzers, *ACS Appl. Mater. Interfaces*, 2021, **13**(14), 16182–16196. Available from: https://pubs.acs.org/doi/10.1021/acsami.0c20690.

8 M. C. Yasin, M. Johar, A. Gupta and S. Shahgaldi, A comprehensive review of the material innovations and corrosion mitigation strategies for PEMWE bipolar plates, *Int. J. Hydrogen Energy*, 2024, **88**, 726–747. Available from: https://linkinghub.elsevier.com/retrieve/pii/S036031992403917X.

9 L. Moradizadeh, P. V. Madhavan, Y. M. Chellehbari, A. Gupta, X. Li and S. Shahgaldi, Porous transport layers with low Pt loading having Nb–Ta alloy as interlayer for proton exchange membrane water electrolyzers, *Int. J. Hydrogen Energy*, 2024, **94**, 1114–1129. Available from: https://linkinghub.elsevier.com/retrieve/pii/S0360319924048742.

10 S. Zaman, M. Khalid and S. Shahgaldi, Advanced Electrocatalyst Supports for Proton Exchange Membrane Water Electrolyzers, *ACS Energy Letters*, 2024, **9**(6), 2922–2935. Available from: https://pubs.acs.org/doi/10.1021/acsenergylett.4c00275.

11 H. M. Irshad and S. Shahgaldi, Comprehensive review of bipolar plates for proton exchange membrane fuel cells with a focus on materials, processing methods and characteristics, *Int. J. Hydrogen Energy*, 2025, **111**, 462–487. Available from: https://linkinghub.elsevier.com/retrieve/pii/S036031992500878X.

12 M. Prestat, Corrosion of structural components of proton exchange membrane water electrolyzer anodes: A review, *J. Power Sources*, 2023, **556**(2022), 232469. Available from: https://doi.org/10.1016/j.jpowsour.2022.232469.

13 H. Q. Fan, Y. M. Wu, S. Su, D. D. Shi, X. Z. Wang and Y. Behnamian, *et al.*, Solution acidity and temperature induced anodic dissolution and degradation of through-plane electrical conductivity of Au/TiN coated metal bipolar plates used in PEMFC, *Energy*, 2022, **254**, 124453. Available from: https://doi.org/10.1016/j.energy.2022.124453.

14 S. Stiber, N. Sata, T. Morawietz, S. A. Ansar, T. Jahnke and J. K. Lee, *et al.*, A high-performance, durable and low-cost proton exchange membrane electrolyser with stainless steel

components, *Energy Environ. Sci.*, 2022, **15**(1), 109–122. Available from: https://xlink.rsc.org/?DOI=D1EE02112E.

15 Q. Feng, X. Yuan, G. Liu, B. Wei, Z. Zhang and H. Li, *et al.*, A review of proton exchange membrane water electrolysis on degradation mechanisms and mitigation strategies, *J. Power Sources*, 2017, **366**, 33–55. Available from: https://doi.org/10.1016/j.jpowsour.2017.09.006.

16 C. Wang and L. Feng, Recent advances and perspectives of Ir-based anode catalysts in PEM water electrolysis, *Energy Adv.*, 2024, **3**(1), 14–29. Available from: https://xlink.rsc.org/?DOI=D3YA00492A.

17 A. Z. Tomić, I. Pivac and F. Barbir, A review of testing procedures for proton exchange membrane electrolyzer degradation, *J. Power Sources.*, 2023, **557**(2022), 232569. Available from: https://linkinghub.elsevier.com/retrieve/pii/S0378775322015464.

18 L. Moradizadeh, P. V. Madhavan, A. Ozden, X. Li and S. Shahgaldi, Advances in protective coatings for porous transport layers in proton exchange membrane water electrolyzers: Performance and durability insights, *Energy Convers. Manage.*, 2025, **332**, 119713. Available from: https://linkinghub.elsevier.com/retrieve/pii/S0196890425002365.

19 R. Vinodh, T. Palanivel, S. S. Kalanur and B. G. Pollet, Recent advancements in catalyst coated membranes for water electrolysis: a critical review, *Energy Adv.*, 2024, **3**(6), 1144–1166. Available from: https://xlink.rsc.org/?DOI=D4YA00143E.

20 A. Singh, B. S. De, S. Singh, S. P. Thota, M. Khalid and S. Shahgaldi, Exploring the engineered electroplating process for coating of gold on the inner structure of porous transport layer (PTL): Performance evaluation of coating in simulated PEM electrolyzer, *Int. J. Hydrogen Energy*, 2025, **106**, 1029–1040. Available from: https://linkinghub.elsevier.com/retrieve/pii/S0360319925006123.

21 C. Liu, M. Carmo, G. Bender, A. Everwand, T. Lickert and J. L. Young, *et al.*, Performance enhancement of PEM electrolyzers through iridium-coated titanium porous transport layers, *Electrochem. Commun.*, 2018, **97**, 96–99. Available from: https://linkinghub.elsevier.com/retrieve/pii/S1388248118302741.

22 T. L. Doan, H. E. Lee, S. S. H. Shah, M. Kim, C. Kim and H. Cho, *et al.*, A review of the porous transport layer in polymer electrolyte membrane water electrolysis, *Int. J. Energy Res.*, 2021, **45**(10), 14207–14220. Available from: https://onlinelibrary.wiley.com/doi/10.1002/er.6739.

23 A. Gupta, Y. M. Chellehbari and S. Shahgaldi, Achieving high performance and durability with ultra-low precious metal nanolayer on porous transport layer for PEMWE application, *J. Power Sources*, 2025, **630**, 236088. Available from: https://linkinghub.elsevier.com/retrieve/pii/S0378775324020408.

24 Anurag, A. Gupta and S. Shahgaldi, An experimental approach to reduce precious metal loading on porous transport layer by using magnetron sputtering method for PEMWE application, *Electrochim. Acta*, 2025, **538**, 147053. Available from: https://doi.org/10.1016/j.electacta.2025.147053.

25 G. Yang, S. Yu, J. Mo, Z. Kang, Y. Dohrmann and F. A. List, *et al.*, Bipolar plate development with additive manufacturing and protective coating for durable and high-efficiency hydrogen production, *J. Power Sources*, 2018, **396**, 590–598. Available from: https://doi.org/10.1016/j.jpowsour.2018.06.078.

26 X. Z. Wang, M. M. Zhang, D. D. Shi, S. C. Zhang, Y. M. Wu and W. J. Gong, *et al.*, Long-term polarization accelerated degradation of nano-thin C/Ti coated SS316L bipolar plates used in polymer electrolyte membrane fuel cells, *Int. J. Hydrogen Energy*, 2022, **47**(14), 8974–8992. Available from: https://doi.org/10.1016/j.ijhydene.2021.12.229.

27 T. Srour, K. Kumar, V. Martin, L. Dubau, F. Maillard and B. Gilles, *et al.*, On the contact resistance between the anode and the porous transport layer in a proton exchange membrane water electrolyzer, *Int. J. Hydrogen Energy*, 2024, **58**, 351–361. Available from: https://linkinghub.elsevier.com/retrieve/pii/S036031992400137X.

28 Z. Kang, J. Mo, G. Yang, Y. Li, D. A. Talley and S. T. Retterer, *et al.*, Thin film surface modifications of thin/tunable liquid/gas diffusion layers for high-efficiency proton exchange membrane electrolyzer cells, *Appl. Energy*, 2017, **206**, 983–990. Available from: https://linkinghub.elsevier.com/retrieve/pii/S030626191731276X.

29 C. Liu, M. Shviro, A. S. Gago, S. F. Zaccarine, G. Bender and P. Gazdzicki, *et al.*, Exploring the Interface of Skin-Layered Titanium Fibers for Electrochemical Water Splitting, *Adv. Energy Mater.*, 2021, **11**(8), 2002926, Available from: https://advanced.onlinelibrary.wiley.com/doi/10.1002/aenm.202002926.

30 S. Singh, A. Singh, M. A. Iqbal and S. Shahgaldi, Constructing an ultra-low loading of IrPt bimetallic coated porous transport layer (PTL) for a PEM water electrolyzer application, *Int. J. Hydrogen Energy*, 2025, **157**, 150478. Available from: https://linkinghub.elsevier.com/retrieve/pii/S0360319925034779.

31 T. Bautkinova, N. Utsch, T. Bystron, M. Lhotka, M. Kohoutkova and M. Shviro, *et al.*, Introducing titanium hydride on porous transport layer for more energy efficient water electrolysis with proton exchange membrane, *J. Power Sources.*, 2023, **565**(1), 232913. Available from: https://www.sciencedirect.com/science/article/pii/S0378775323002884?via%3Dihub.

32 L. Stein, A. Dittrich, D. C. Walter, P. Trinke, B. Bensmann and R. Hanke-Rauschenbach, Degradation of PGM and PGM-free Coatings on PEMWE Porous Transport Layers, *ACS Appl. Mater. Interfaces*, 2025, **17**(12), 19070–19085. Available from: https://pubs.acs.org/doi/10.1021/acsami.4c22455.

33 S. Cherevko, A. R. Zeradjanin, G. P. Keeley and K. J. J. J. Mayrhofer, A Comparative Study on Gold and Platinum Dissolution in Acidic and Alkaline Media, *J. Electrochem. Soc.*, 2014, **161**(12), H822–H830. Available from: https://iopscience.iop.org/article/10.1149/2.0881412jes.

34 W. Giurlani, G. Zangari, F. Gambinossi, M. Passaponti, E. Salvietti and F. Di Benedetto, *et al.*, Electroplating for Decorative Applications: Recent Trends in Research and

Development, *Coatings*, 2018, **8**(8), 260. Available from: https://www.mdpi.com/2079-6412/8/8/260.

35 J. H. Choi, H. Eun Kang, D. J. Kim and Y. Soo Yoon, A Comprehensive Review of Stainless-Steel Bipolar Plate Coatings and Their Role in Mitigating Corrosion in Aggressive Proton-Exchange Membrane Fuel Cells Environments, *Chem. Eng. J.*, 2024, **493**, 152662. Available from: https://linkinghub.elsevier.com/retrieve/pii/S1385894724041494.

36 J. Liang, Q. Liu, T. Li, Y. Luo, S. Lu and X. Shi, *et al.*, Magnetron sputtering enabled sustainable synthesis of nanomaterials for energy electrocatalysis, *Green Chem.*, 2021, **23**(8), 2834–2867.

37 R. Skvorčinskienė, M. Urbonavičius, L. Vorotinskienė, M. Bašinskas, K. Zakarauskas and M. Maziukienė, *et al.*, Application of TiH_2 dehydrogenation for vapour layer formation under boiling crisis conditions, *Appl. Ther. Eng.*, 2024, **247**(2023), 122935. Available from: https://linkinghub.elsevier.com/retrieve/pii/S1359431124006033.

38 M. J. Frank, M. S. Walter, S. P. Lyngstadaas, E. Wintermantel and H. J. Haugen, Hydrogen content in titanium and a titanium–zirconium alloy after acid etching, *Mater. Sci. Eng. C*, 2013, **33**(3), 1282–1288. Available from: https://linkinghub.elsevier.com/retrieve/pii/S092849311200584X.

39 P. Lettenmeier, R. Wang, R. Abouatallah, B. Saruhan, O. Freitag and P. Gazdzicki, *et al.*, Low-Cost and Durable Bipolar Plates for Proton Exchange Membrane Electrolyzers, *Sci. Rep.*, 2017, **7**(1), 44035. Available from: https://www.nature.com/articles/srep44035.

40 Z. Lei, T. Wang, B. Zhao, W. Cai, Y. Liu and S. Jiao, *et al.*, Recent Progress in Electrocatalysts for Acidic Water Oxidation, *Adv. Energy Mater.*, 2020, **10**(23), 1–18.

41 K. J. Ferner and S. Litster, Composite Anode for PEM Water Electrolyzers: Lowering Iridium Loadings and Reducing Material Costs with a Conductive Additive, *ACS Appl. Energy Mater.*, 2024, **7**(18), 8124–8135. Available from: https://pubs.acs.org/doi/10.1021/acsaem.4c01866.

42 Y. Liu, S. Huang, D. Wang, H. Zhang, D. Shan and S. Peng, *et al.*, Modifying Ti-Based Gas Diffusion Layer Passivation for Polymer Electrolyte Membrane Water Electrolysis via Electrochemical Nitridation, *ACS Appl. Mater. Interfaces*, 2022, **14**(13), 15728–15735. Available from: https://pubs.acs.org/doi/10.1021/acsami.1c22639.

43 T. Bystron, M. Vesely, M. Paidar, G. Papakonstantinou, K. Sundmacher and B. Bensmann, *et al.*, Enhancing PEM water electrolysis efficiency by reducing the extent of Ti gas diffusion layer passivation, *J. Appl. Electrochem.*, 2018, **48**(6), 713–723. Available from: https://link.springer.com/10.1007/s10800-018-1174-6.

44 S. Trasatti, Work function, electronegativity, and electrochemical behaviour of metals. III. Electrolytic hydrogen evolution in acid solutions, *J. Electroanal. Chem.*, 1972, **39**(1), 163–184.

45 M. Johar, L. Moradizadeh, A. Gupta, Y. Mehdizadeh Chellehbari, X. Li and S. Shahgaldi, Development of novel Nb and Ta multilayer coatings for corrosion protection of Ti-based bipolar plates for proton exchange membrane fuel cells, *Corros. Sci.*, 2025, **245**, 112707. Available from: https://linkinghub.elsevier.com/retrieve/pii/S0010938X25000344.

46 G. Tremiliosi-Filho, L. H. Dall'Antonia and G. Jerkiewicz, Growth of surface oxides on gold electrodes under well-defined potential, time and temperature conditions, *J. Electroanal. Chem.*, 2005, **578**(1), 1–8. Available from: https://linkinghub.elsevier.com/retrieve/pii/S0022072804006400.

47 S. Cherevko, A. A. Topalov, I. Katsounaros and K. J. J. Mayrhofer, Electrochemical dissolution of gold in acidic medium, *Electrochem. Commun.*, 2013, **28**, 44–46. Available from: https://linkinghub.elsevier.com/retrieve/pii/S1388248112005310.

48 X. Gao, G. Xu, Y. Zhao, S. Li, F. Shi and Y. Chen, Self-assembly of amine-functionalized gold nanoparticles on phosphonate-functionalized graphene nanosheets: a highly active catalyst for the reduction of 4-nitrophenol, *RSC Adv.*, 2015, **5**(107), 88045–88051. Available from: https://xlink.rsc.org/?DOI=C5RA18228J.

49 Z. Fan, H. Yu, G. Jiang, D. Yao, S. Sun and J. Chi, *et al.*, Low precious metal loading porous transport layer coating and anode catalyst layer for proton exchange membrane water electrolysis, *Int. J. Hydrogen Energy*, 2022, **47**(44), 18963–18971. Available from: https://linkinghub.elsevier.com/retrieve/pii/S0360319922016603.

50 G. Schmidl, J. Dellith, E. Kessler and U. Schinkel, The influence of deposition parameters on Ti/Pt film growth by confocal sputtering and the temperature dependent resistance behavior using SiOx and Al2O3 substrates, *Appl. Surface Sci.*, 2014, **313**, 267–275. Available from: https://linkinghub.elsevier.com/retrieve/pii/S0169433214012446.

51 A. Dorjgotov, Y. Jeon, J. Hwang, B. Ulziidelger, H. S. Kim and B. Han, *et al.*, Synthesis of Durable Small-sized Bilayer Au@Pt Nanoparticles for High Performance PEMFC Catalysts, *Electrochim. Acta*, 2017, **228**, 389–397.

52 M. Geuß, L. Löttert, A. Hutzler, J. Schwarz, J. Nováková and I. Khalakhan, *et al.*, Platinum interlayers reduce charge transport barriers between amorphous Ir-oxide OER electrocatalysts and the porous transport layer, *Chem. Eng. J.*, 2025, **514**, 162887. Available from: https://linkinghub.elsevier.com/retrieve/pii/S1385894725037131.

53 S. Geiger, O. Kasian, M. Ledendecker, E. Pizzutilo, A. M. Mingers and W. T. Fu, *et al.*, The stability number as a metric for electrocatalyst stability benchmarking, *Nat. Catal.*, 2018, **1**(7), 508–515.

54 C. Rakousky, G. P. Keeley, K. Wippermann, M. Carmo and D. Stolten, The stability challenge on the pathway to high-current-density polymer electrolyte membrane water electrolyzers, *Electrochim. Acta*, 2018, **278**, 324–331. Available from: https://linkinghub.elsevier.com/retrieve/pii/S0013468618309150.

55 S. A. Grigoriev, P. Millet, S. A. Volobuev and V. N. Fateev, Optimization of porous current collectors for PEM water electrolysers, *Int. J. Hydrogen Energy*, 2009, **34**(11), 4968–4973. Available from: https://linkinghub.elsevier.com/retrieve/pii/S0360319908015528.

56 M. Yasutake, Z. Noda, J. Matsuda, S. M. Lyth, M. Nishihara and K. Ito, *et al.*, Ru-core Ir-shell electrocatalysts deposited on a surface-modified Ti-based porous transport layer for polymer electrolyte membrane water electrolysis, *Int. J. Hydrogen Energy*, 2024, **49**, 169–183. Available from: https://linkinghub.elsevier.com/retrieve/pii/S0360319923034419.

57 J. O. Majasan, F. Iacoviello, P. R. Shearing and D. J. L. Brett, Effect of microstructure of porous transport layer on performance in polymer electrolyte membrane water electrolyser, *Energy Procedia*, 2018, **151**, 111–119.

58 T. Lickert, S. Fischer, J. L. Young, S. Klose, I. Franzetti and D. Hahn, *et al.*, Advances in benchmarking and round robin testing for PEM water electrolysis: Reference protocol and hardware, *Appl. Energy*, 2023, **352**, 121898. Available from: https://linkinghub.elsevier.com/retrieve/pii/S030626192301262X.

59 H. Ito, T. Maeda, A. Nakano and H. Takenaka, Properties of Nafion membranes under PEM water electrolysis conditions, *Int. J. Hydrogen Energy*, 2011, **36**(17), 10527–10540. Available from: https://linkinghub.elsevier.com/retrieve/pii/S0360319911013760.

60 M. Suermann, T. J. Schmidt and F. N. Büchi, Cell Performance Determining Parameters in High Pressure Water Electrolysis, *Electrochim. Acta*, 2016, **211**, 989–997. Available from: https://linkinghub.elsevier.com/retrieve/pii/S0013468616314372.

61 A. Kosakian, L. P. Urbina, A. Heaman and M. Secanell, Understanding single-phase water-management signatures in fuel-cell impedance spectra: A numerical study, *Electrochim. Acta*, 2020, **350**, 136204. Available from: https://linkinghub.elsevier.com/retrieve/pii/S001346862030596X.

62 C. Immerz, B. Bensmann, P. Trinke, M. Suermann and R. Hanke-Rauschenbach, Local Current Density and Electrochemical Impedance Measurements within 50 cm Single-Channel PEM Electrolysis Cell, *J. Electrochem. Soc.*, 2018, **165**(16), F1292–F1299. Available from: https://iopscience.iop.org/article/10.1149/2.0411816jes.

63 M. Schönleber, D. Klotz and E. Ivers-Tiffée, A Method for Improving the Robustness of linear Kramers-Kronig Validity Tests, *Electrochim. Acta*, 2014, **131**, 20–27. Available from: https://linkinghub.elsevier.com/retrieve/pii/S0013468614001005.

64 B. A. Boukamp, A Linear Kronig-Kramers Transform Test for Immittance Data Validation, *J. Electrochem. Soc.*, 1995, **142**(6), 1885–1894. Available from: https://iopscience.iop.org/article/10.1149/1.2044210.

65 A. Z. Tomić, I. Pivac and F. Barbir, Impact of power profile on activation of proton exchange membrane electrolyzer cell, *J. Power Sources*, 2025, **632**(2024), 236308. Available from: https://linkinghub.elsevier.com/retrieve/pii/S0378775325001442.